Closed loop control of a magnetic particle at the air/liquid interface

Mohamed Dkhil[1,2], Mohamed Kharboutly[1],
Aude Bolopion[1], Stéphane Régnier[2], *Member, IEEE,* Michaël Gauthier[1], *Member, IEEE*

***Abstract*—One of the greatest challenges in microrobotic is the development of robotic devices for high speed transportation and precise positioning of microcomponents. This paper proposes to use non contact magnetic actuation in which objects are placed at the air/liquid interface and are actuated through magnetic field gradients. A physical model is developed and identified to perform closed loop control. This approach is validated through several experiments in 1D. Precise positioning and high speed trajectory tracking of objects smaller than 100 μm are achieved. The position error of an object of 60x50x25 μm^3 is less than 10 % of its size and the maximum velocity reached is about 6 mm/s. The closed loop control has been tested on objects as small as 30x20x25 μm^3 and demonstrates its ability to perform precise positioning (the position error is less than 7 % of the size of the object). This approach represents a promising solution to design devices for high throughput transportation and precise positioning of micro-objects, which will lead to magnetic smart surfaces at micrometer scale.**

***Note to Practitioners*— This paper was motivated by the problem of the adhesion effects on the control of objects at the microscale. The micro-objects behave differently in ambient environments and in liquids. In ambient environments the micro-objects can reach high velocities since the viscous forces are negligible, however the adhesion forces limit the repeatability of the motion. In liquid medium the issues of the adhesion effect decrease, but the velocity is limited due to the viscous forces. This paper suggests a non contact approach where micro-objects are placed at the air/liquid interface and are controlled by magnetic forces. In this paper, we have demonstrated by using a closed loop control a high speed and precise actuation of micro-objects along one axis (1D). The position error of an object of 60x50x25 μm^3 is less than 10 % of its size and the maximum velocity reached is about 6 mm/s. In addition, objects smaller than 50 μm can be controlled (the position error of an object of 30x20x25 μm^3 is less than 7 % of its size). This approach avoids the issues of the adhesion effects and represents a promising solution for high speed transportation and precise positioning of objects. In future research, a strategy of control will be developed for high speed/precise control of objects in 2D. These developments will directly contribute to the design of magnetic smart surfaces at micrometer scale that will convey microcomponents. It represents a key element of future assembly lines at micrometer scale.**

***Index Terms*—Air/liquid interface, objects, magnetic field gradient, high speed, precise positioning.**

[1]Authors are with FEMTO-ST Institute CNRS UFC/ENSMM/UTBM Automatic Control and Micromechatronic Systems Department, 24 rue Alain Savary, 25000 Besançon, France. mohamed.dkhil@femto-st.fr

[2]Authors are with Institut des Systèmes Intelligents et de Robotique (ISIR), Pierre et Marie Curie University, CNRS UMR 7222, 4 Place Jussieu, 75005 Paris, France.

I. Introduction

Smart surfaces are well studied solutions to manipulate, convey, and position objects of a few millimeters in the plan [1], [2], [3]. For industrial tasks such as the assembly and the packaging of products automatic feeding of objects is crucial. These methods enable to manipulate the objects with no direct contact which avoids damages of fragile components such as electronic cards. As the size of these industrial objects decreases there will be an urgent need for miniaturized smart surfaces in order to manipulate objects of a few micrometers. To ensure the displacement of objects at the microscale, some non contact actuation techniques can be exploited. The micro-objects can be moved without any direct contact and can reach a high velocity because of the negligible inertia effect at this scale. Several actuation techniques are available to control micrometer size objects, such as magnetic actuation [4], [5], [6]; dielectrophoresis [7], [8], [9], [10]; laser tweezers [11], [12], [13] or acoustic waves [14], [15].

Magnetic energy is a promising solution to actuate objects with high speed. Today, there is a significant trend towards the use of this actuation principle [4], [16], [17]. A wide range of microrobots are controlled using several coils or electromagnets [18], [19], [20], [21], [22], [23]. To give only a few examples, helical microrobots are moved using a rotating magnetic field [24], [25]; some bacteria such as Tetrahymena pyriformis are actuated by magnetic field and used as microrobots [26], [27], [28]. This success can be attributed to the ability of magnetic actuation to produce fast displacements. Magnetic stick-slip motion is used in [29] to actuate a ferromagnetic object of 250x130x10 μm^3 with a velocity higher than 10 mm/s. However, the rocking behavior cannot ensure a precise positioning of the micro-object. A rectangular micro-object of size 388x388x230 μm^3 is presented in [30] and demonstrates a velocity higher than 133 mm/s, but the adhesion between the micro-object and the substrate limits the repeatability of the behavior. Other works focus on the control of smaller objects. Paramagnetic microparticles with an average diameter of 100 μm are controlled in the plane [31], [32], [33] and in 3D avoiding obstacle [34], [35]. These works demonstrate an average velocity of 279 μm/s with an average position tracking error of 48 ± 59 μm [36]. Magnetic helical swimmer of 42 μm length and 6 μm of diameter is presented in [37] and demonstrates a maximum velocity of 300 μm/s and a position

error of 30 μm. A sperm-shaped microrobot presented in [38] can swim using flagella propulsion with a velocity of 21 μm/s and a position error of 20 μm. The systems presented above are either in ambient environments or in liquids. However at micrometer scale adhesion forces are a major issue in ambient environments, and the repeatability of the control is not guaranteed [39]. In liquid medium the issues of the adhesion effect decrease due to the absence of capillarity and the reduction of the electrostatic interaction [40]. This medium ensures the repeatability of the object's behavior but the velocity is limited due to the viscous forces.

To go beyond the performances of current systems, this paper focuses on object control at the air/liquid interface. Indeed, many works demonstrate an interesting applications of the use of the fluid/fluid interface. By varying the interfacial tension, it is possible to control the assembly of gold nanoparticles [41] or gears [42]. Selective particle clustering at the air/liquid interface is demonstrated in [43]. An other work demonstrates the ability to create a surface vortex pump by a fast rotation of several micro-beads. This method can be used to measure the surface viscosity and to perform size-selective sorting of micro-objects [44]. The fluid/fluid interface is also of interest for microrobotics: a magnetically actuated microrobot of typical size of 200 μm has been controlled in 2D at the interface between oil and sodium bicarbonate solution. However it demonstrates a low velocity of 23 μm/s [45].

In this paper it is shown that microrobots can reach high velocities at the air/liquid interface. The actuation is ensured by magnetic forces. The object is in equilibrium on the interface under the action of the surface tension and its weight, and it moves on the surface with minimum friction. A proof-of-concept was introduced in [46], where initial open loop experimental results were discussed and closed loop control has been performed in [45] but only low velocities have been achieved (less than 23 μm/s). In this present work, closed loop control is proposed based on a model of the system. Experimental results validate this approach in 1D through precise positioning and trajectory tracking tests on objects smaller than 100 μm.

This paper is organized as follows. In Section II, the behavior of a micro-object at the air/liquid interface is characterized by several experiments in open loop. A simplified analytical model is developed in Section III. In Section IV, the physical parameters of the model are experimentally identified and its validity is discussed. In Section V closed loop control is demonstrated in 1D. Experiments involving objects of less than 100 μm are presented. The advantages and limitations of this approach are discussed in Section VI. Conclusions and perspectives of this work are presented in the last section.

II. Analysis of the influence of environmental conditions on open loop control

In this section the motion of an object at the air/liquid interface in open loop is presented and the different sources of disturbances acting on the behavior of this object are identified.

A. Open loop control

The proposed approach consists in actuating magnetic objects at the air/liquid interface using four electromagnets (see Figure 1). Currently, the proposed magnetic actuation systems are used to manipulate ferromagnetic, paramagnetic or diamagnetic objects. When a magnetic field gradient is applied, diamagnetic objects present a low magnetization and are repelled from the magnetic sources ensuring a final stable equilibrium. On the contrary, ferromagnetic and paramagnetic objects are attracted toward the magnetic sources which induces an unstable dynamic behavior. However, in this work, the particles are placed at the air/liquid interface having a meniscus shape. Due to this particular shape of the surface the system is not inherently unstable even while using ferromagnetic or paramagnetic particles. To benefit from high forces and high velocities ferromagnetic material is chosen since its magnetization is higher than the one of paramagnetic and diamagnetic objects [30].

The two pairs of electromagnets enable to control in-plane displacements. The workspace is a cylindrical reservoir which is small (up to some millimeters) located in the center of the magnetic actuation device. At this scale a concave meniscus with a curvature radius R_c appears on the reservoir. The micro-object is placed initially at the center of the meniscus (Figure 2). It is in equilibrium on the interface under the action of the resultant force of surface tension $\vec{T}$ and its weight $\vec{P}$ [46]. If one electromagnet is activated by applying a constant value of current I, the magnetic force $\vec{F}_{mag}$ attracts the micro-object which moves on the meniscus surface. A viscous force is created because of the contact between the micro-object and the liquid surface. The micro-object reaches a final position X_∞ when the projection along the $(o,\vec{x})$ axis of the resultant force of surface tension $\vec{T}$ and the magnetic force $\vec{F}_{mag}$ are in equilibrium (see Figure 2). In Section III, a physical model will indeed demonstrate that the behavior of the micro-object is given by a first-order system characterized by the response time τ and the final position X_∞. When the magnetic force is switched off, the object goes back to the center of the workspace under the action of gravity.

B. Experimental setup

Several factors can affect the repeatability of the micro-object's behavior among which external disturbances such as dust and vibrations, or the variations of the shape of the meniscus. In the following the repeatability of the motion is discussed considering objects having different sizes. In order to identify these disturbance sources the following experimental setup is used (see Figure 3). To minimize the mechanical noise the magnetic device is placed on an antivibration base (Newport SG Breadboard). Nickel micro-objects with a rectangular shape are fabricated using micro-fabrication technologies. Nickel electrodeposition is performed on a silicon wafer. The thickness of the nickel layer is around 25 μm.

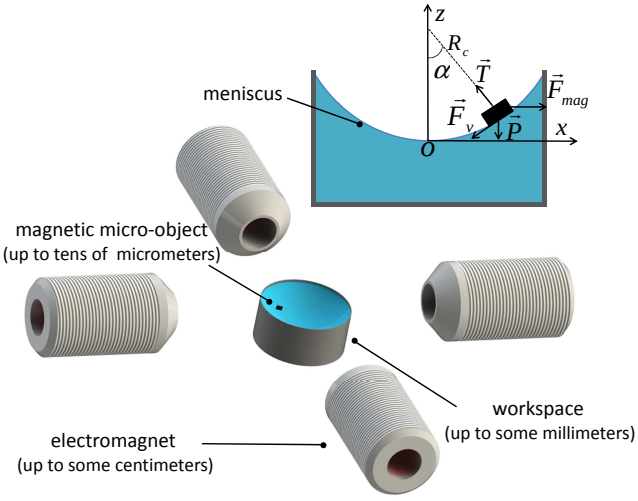

Fig. 1: Conceptual view of a planar magnetic device. The electromagnets control the motion of the micro-object on the air/liquid interface. R_c is the curvature radius of the meniscus and α is the angle between the vertical direction and the normal to the micro-object. The forces applied to the micro-object are the magnetic force $\vec{F}_{mag}$, the weight $\vec{P}$, the resultant force of surface tension $\vec{T}$ of the air/liquid interface and the viscous force $\vec{F}_v$.

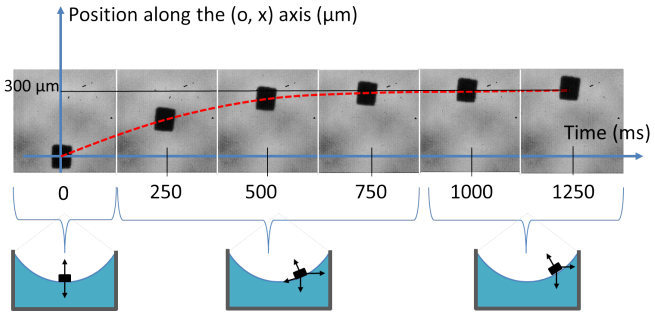

Fig. 2: Trajectory of the micro-object on the air/water interface. At the time $t = 0$ s the micro-object is on the workspace center. When the electromagnet is activated (located at the top of the images), the magnetic force attracts the micro-object which moves on the meniscus surface. At the time $t = 1000$ ms the micro-object reaches an equilibrium position.

To ensure the electrical conductivity for the electrodeposition process a thin layer (hundreds of nanometers) of chromium-nickel is sputtered on the wafer. The objects are then released from the wafer by applying a mechanical effort on each of them. One of these micro-objects is placed on an air/water interface (distilled water is used). Acquisition of images is performed by a "Photonfocus" camera mounted on Mitutoyo M plan Apo 5X objective, which has a depth of field of 14 µm. The maximum resolution of the camera is 1024×1024 pixels with ROI technology (Region of Interest) and a frame rate of 1000 f/s. The field of view of the camera is 2048×2048µm (one pixel represents 2 µm). The reservoir used is 4 mm of diameter. Only the central part of the reservoir is recorded by the camera. The images are imported to a computer using a PCI interface. The PC runs software on a real time Unix Kernel. The software is written in C using OpenCV libraries for image processing. It controls the signals sent to the electromagnets via a National instrument card (NI-PCI-6733). The four electromagnets are placed on a mobile support to adapt the relative position between the workspace and each electromagnet. They are powered by an electronic amplifier (ST TL048CN) which amplifies the control signals issued from the NI card with a response time equal to 0.1 µs. In order to determine the values of the magnetic field measurements were performed using a teslameter (F.W Bell, Model 7010) which is based on the use of a Hall probe to measure the intensity of the magnetic field. The distance between the electromagnet and the probe is controlled by a 3-axis manual manipulator (Newport Corporation). The measurements are made for a step of 250 µm and for different values of current. The obtained data are presented in [46].

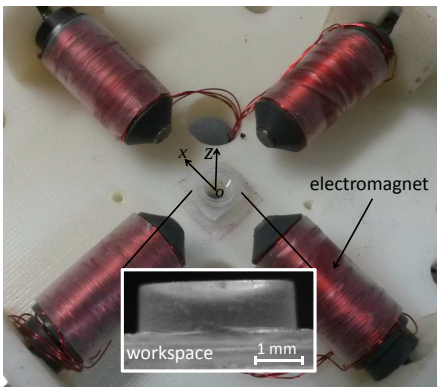

Fig. 3: Experimental setup. The inlet represents the cylindrical workspace used (diameter: 4 mm). The meniscus formed is spherical. The object is placed on the air/liquid interface.

C. *Impact of the object size on its behavior*

To evaluate the impact of the size of the object on its behavior, experiments are performed on three objects having different sizes (large (100x90x25 µm^3), medium (60x50x25 µm^3) and small (30x50x25 µm^3)). So that experiments can be comparable for the three different object sizes a protocol has been defined to get similar filling of the reservoir. Distilled water is poured until it reaches the top of the reservoir. The micro-object is placed on the center of the reservoir. A heating element is placed under the reservoir to evaporate water during 15 min. The obtained radius of curvature of the meniscus has been measured one time to 10.5 mm using a side view camera. It is considered similar for all the experiments. The duration of the overall experiment, which consists in several back and forth movements of the particle, is short enough (less than 2 min) so that it can be considered that the meniscus does not vary (there is no

evaporation during the experiment).

One electromagnet is powered to create the magnetic force. The magnitude of the current used is adapted according to the size of the object. It is set to 0.47 A for the large and medium objects (which corresponds to 0.48 T/m) and to 0.7 A for the small object (which corresponds to 0.69 T/m). Since the small particle is more sensitive to perturbations a higher current (and thus a higher magnetic gradient) must be used to reach the final position set to 300 µm. This particular position has been chosen in order to use the whole field of view of the camera. The time interval of the plots is adjusted so that the transient phase can be correctly seen.

Figure 4(a) (resp. Fig. 4(b) and Fig. 4(c)) presents the response of the large (resp. medium and small) size objects for each trial. The mean value and the standard deviation of the steady state position and the response time are given in the caption. Even if the current used are not the same it can still be concluded that the small particles are more sensitive to perturbations than larger ones. Indeed, even if the small particle experiences a higher magnetic gradient than the large ones the plots of Fig. 4(c) show a less repeatable behavior.

D. Impact of the meniscus variations on the behavior of micro-objects

Due to the small size of the reservoir (up to some millimeters) a concave meniscus appears. Since the reservoir has to be re-filled periodically due to the evaporation of the water it is not possible to guarantee the same shape of the meniscus. Indeed, a capillary hysteresis phenomenon is produced by chemical imperfections and the roughness of the container material. The contact angle between the surface of the container and the liquid is not the same when re-filling the container. It varies between an advancing angle and a receding angle [47], [48], [49]. The increase of the liquid temperature reduces the surface tension and also modifies the contact angle, but its influence is less important than the one of the capillary hysteresis [50]. To limit the inaccuracies the following procedure has been defined: the workspace is completely filled with distilled water. The micro-object is placed on the center of the workspace. A heating element is placed 15 minutes under the workspace to evaporate partially the water and generate the final meniscus shape. To evaluate the impact of the variability of the meniscus geometry on the repeatability of the micro-object behavior, the same five trials as in the previous section (Sec. II-C) are performed. After each group of five trials the workspace is emptied and re-filled. These experiments are performed on the largest object (100x90x25 μm^3) and the medium size one (60x50x25 μm^3). Results are given in Figure 5. These plots can be compared to the ones of Figure 4 performed for a constant meniscus. It can be seen that the repeatability is decreased when the meniscus varies. Despite all the efforts made to get a similar shape of the meniscus it is not possible to guarantee a precise positioning of the micro-object in open loop mode. Thus, a closed loop control is necessary for precise positioning requiring the relation between the input of the system (the current I sent to the electromagnet) and the output of the

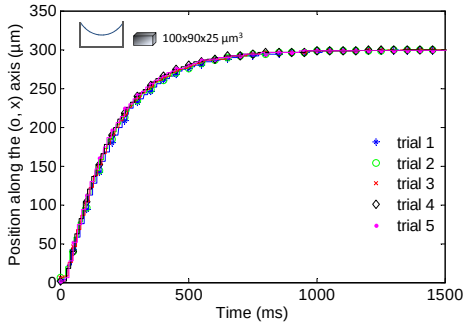

(a) Large size object. The position response demonstrates a repeatable behavior. The current $I = 0.47$ A is applied for 1.5 s. The average values of the steady state position and the response time are respectively $\overline{X_\infty} = 300$ µm and $\overline{\tau} = 187$ ms and the standard deviations are $\sigma_{(X_\infty)} = 1$ µm and $\sigma_{(\tau)} = 3$ ms

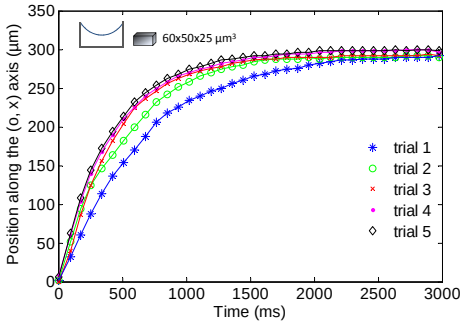

(b) Medium size object. The position response demonstrates a less repeatable behavior. The current $I = 0.47$ A is applied for 3 s. The average values of the steady state position and the response time are respectively $\overline{X_\infty} = 296$ µm and $\overline{\tau} = 433$ ms and the standard deviations are $\sigma_{(X_\infty)} = 1$ µm and $\sigma_{(\tau)} = 12$ ms.

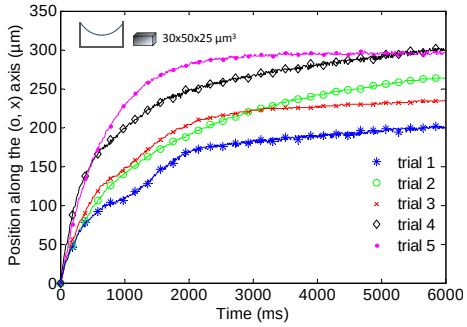

(c) Small size object. The position response demonstrates a non repeatable behavior. The current $I = 0.7$ A is applied for 6 s. The average values of the steady state position and the response time are respectively $\overline{X_\infty} = 259$ µm and $\overline{\tau} = 1129$ ms and the standard deviations are $\sigma_{(X_\infty)} = 37$ µm and $\sigma_{(\tau)} = 293$ ms.

Fig. 4: Position response of different size objects. Five different trials are performed. It can be seen that as its size decreases the trajectory of the object becomes less repeatable.

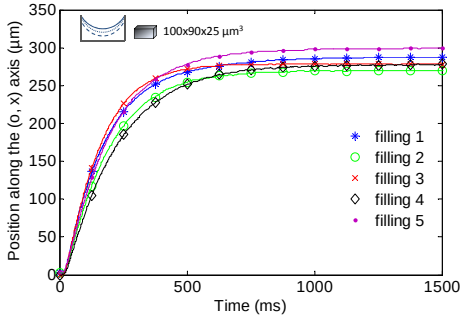

(a) Large size object. The position response demonstrates the impact of the meniscus variations on its behavior. The current $I = 0.47$ A is applied for 1.5 s. The average values of the steady state position and the response time are respectively $\overline{X_\infty} = 283$ µm and $\overline{\tau} = 174$ ms and the standard deviations are $\sigma_{(X_\infty)} = 12$ µm and $\sigma_{(\tau)} = 6$ ms.

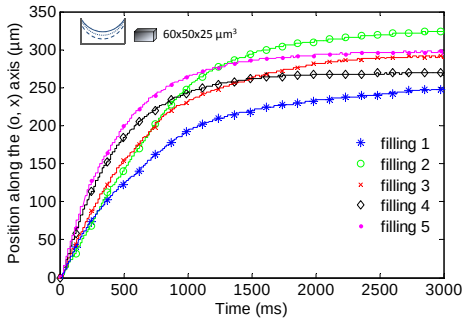

(b) Medium size object. The position response demonstrates the impact of the meniscus variations on its behavior. The current $I = 0.47$ A is applied for 3 s. The average values of the steady state position and the response time are respectively $\overline{X_\infty} = 287$ µm and $\overline{\tau} = 450$ ms and the standard deviations are $\sigma_{(X_\infty)} = 16$ µm and $\sigma_{(\tau)} = 31$ ms.

Fig. 5: Position response for different radius of curvature R_c of the meniscus. Five trials are performed and the results are averaged. The reservoir is then refilled and five new trials are performed for both the large and the medium size objects (this is done for five different fillings). The workspace is refilled between each group of five trials, thus the shape of the meniscus is slightly different for each group. The trajectory of the object depends on the meniscus shape.

system (the position x of the micro-object). Thus, a model of a micro-object's behavior is proposed in the next section.

III. Dynamic Model

Firstly, the model of motion of an object on the (x,z) plane is presented. Secondly, the model of motion along the $(o,\vec{x})$ axis will be developed and used to perform closed loop control of the position of the objects in 1D (along the $(o,\vec{x})$ axis).

A. Model of the motion of a micro-object at the air/liquid interface

The micro-object is placed at the air/liquid interface. The workspace is small (up to some millimeters), a meniscus appears on the reservoir, which must be taken into account while modeling the motion (see Figure 1). The shape of the meniscus can be a concave surface depending on the material properties of the reservoir. It is defined by the function f:

$$z = f(x). \tag{1}$$

The weight of the micro-object $\vec{P}$ is compensated by the resultant force of the surface tension $\vec{T}$(see Figure 6). The equilibrium condition is given by:

$$\gamma C \sin(\phi) = mg, \tag{2}$$

where γ is the surface tension, C is the perimeter of the object, ϕ is the contact angle between the micro-object and the liquid, m is the mass of the object and $g = 9.8$ m.s^{-2} is the acceleration of the gravity. To evaluate the deformation of the meniscus due to the presence of the object the ϕ angle is evaluated numerically. A rectangular nickel object is considered (density: $\rho = 8902$ kg/m^3, size: 100x90x25 µm^3) and the liquid is water (surface tension: $\gamma = 72\ 10^{-3}$ N/m). Based on Equation (2) the ϕ angle is about $7.2\ 10^{-4}$ rad which is negligible. The shape of the meniscus is not affected by the weight of the micro-object and Eq. (1) can be used despite the presence of the object.

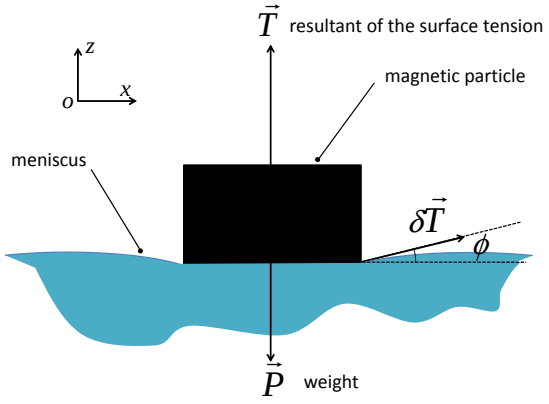

Fig. 6: Equilibrium of the magnetic micro-object on the meniscus. The resultant force of surface tension $\vec{T}$ compensates the weight $\vec{P}$. It can be shown that the contact angle ϕ between the micro-object and the liquid is negligible, therefore, the shape of the meniscus in the reservoir is not significantly deformed by the weight of the micro-object.

The magnetic force $\vec{F}_{mag}$ applied to a magnetic micro-object is given by:

$$\vec{F}_{mag} = V.\nabla(\vec{M}.\vec{B}), \tag{3}$$

where V is the volume of the object, $\vec{M}$ is its magnetization and $\nabla\vec{B}$ is the magnetic field gradient produced by the magnetic source. The response time of the electromagnet is estimated to 352 µs by calculating its electrical inductance and resistance. This value is 500 times smaller than the mechanical response time of objects (around 180 ms for the large object). Thus, the

establishment of the magnetic field is considered instantaneous in this modeling.

The force applied by the surrounding fluids on the object includes the viscous force applied by the air on the front surface of the object and the shear force developed by the contact between the object and the liquid surface. The viscous force applied to the front surface by the air is negligible compared to the shear force due to the difference between the air and the liquid viscosity. The shear force depends on the viscosity of the fluid, the object geometry and the contact angle between the object and the liquid surface [51]. Considering the Stokes law it is expressed by:

$$\vec{F}_v = -h\vec{v}, \tag{4}$$

where h is a viscous coefficient and $\vec{v}$ is the velocity of the object.

Using the second Newton's law, the motion of the micro-object can be expressed as follows:

$$m\vec{a} = \vec{P} + \vec{F}_{mag} + \vec{F}_v + \vec{T}, \tag{5}$$

where $\vec{a}$ is the acceleration of the micro-object and m is its mass. This equation is projected along $(o,\vec{x})$ and $(o,\vec{z})$:

$$\begin{cases} m\ddot{x} = F_{magx} - hv\cos(\alpha) - T\sin(\alpha), \\ m\ddot{z} = F_{magz} - P - hv\sin(\alpha) + T\cos(\alpha), \\ z = f(x), \\ \tan(\alpha) = \dfrac{df(x)}{dx}, \end{cases} \tag{6}$$

where α is the angle between the vertical direction and the normal to the micro-object. The general behavior of the micro-object is given by Eq. (6).

B. Simplified dynamic model

In order to derive a simplified dynamic model for closed loop control, some assumptions will be made:

- The curvature of the meniscus is considered spherical, with a radius R_c. The position x and z are related to R_c and the angle α by:

$$\begin{cases} x = R_c\sin(\alpha), \\ z = R_c(1-\cos(\alpha)), \end{cases} \tag{7}$$

- Only local displacements around the center of the workspace are considered. Thus $\alpha << 1$ and the approximations $\sin(\alpha) \approx \alpha$ and $\cos(\alpha) \approx 1$ are satisfied.
- Due to the small size of the object the inertial terms $m\ddot{x}$ and $m\ddot{z}$ can be neglected in Eq. (6).
- It is considered that the magnetic force applied by the electromagnet on the micro-object is directed along the $(o,\vec{x})$ axis: $F_{magz} = 0$.

The validity of these assumptions will be discussed in Section IV.

Based on the above assumptions the dynamic model simplifies to:

$$h\dot{x} + \left(\frac{mg}{R_c}\right)x = F_{mag}(x,I). \tag{8}$$

The magnetic force is defined by the Eq. (3) as a function of the magnetic field $\vec{B}$. Initially, the micro-object is located at 10 mm distance from the electromagnet and should perform a small displacement (about 300 µm) to reach a distance of 9.7 mm from the electromagnet. In this range of displacement, the magnetic field can be approximated by a constant value 2.9 mT for a current equal to 0.47 A. Concerning the magnetic field gradient, its value varies between a maximum value (0.52 T/m at the position 9.7 mm from the electromagnet) and a minimum value (0.44 T/m at the position 10 mm from the electromagnet). Then it is approximated by the average value (0.48 T/m for $I = 0.47$ A). Considering that there is no saturation of the magnetic core of the coils, the magnetic field gradient can be approximated by the relation:

$$\nabla B = aI, \tag{9}$$

where $a \simeq 1$ T/Am depends on the geometric characteristics of the electromagnet, the number of turns of the wire on the electromagnet and the magnetic constant of the magnetic core. In that case, the magnetic field gradient $\nabla\vec{B}(I)$ and the magnetization $\vec{M}(I)$ depend only on the current I set to the electromagnet. In the following this approximation will be made since the object will remain further than 9 mm away from the electromagnet.
Based on the above results the simplified dynamic model is:

$$h\dot{x} + \left(\frac{mg}{R_c}\right)x = V\left(M(I)\nabla B(I)\right). \tag{10}$$

The dynamic behavior of the micro-object is given by a first order differential equation whose solution depends on the curvature of the meniscus R_c. The steady state position X_∞ can be expressed in function of the magnetization M by:

$$X_\infty = \frac{R_c\left(M(I)\nabla B(I)\right)}{\rho g}, \tag{11}$$

where $m = \rho V$ with ρ the density of the object. In addition the response time τ can be expressed in function of the viscous coefficient h by:

$$\tau = \frac{hR_c}{mg}. \tag{12}$$

The model presents two unknown parameters, namely the viscous coefficient h and the magnetization of the material M. In the next section, a method to identify these parameters will be presented based on the open loop experimental measurements performed on the largest object.

IV. Identification and validation of the model

The analytical relations between I and F_{mag} (Eq. (3)) and between F_{mag} and x (Eq. (8)) define the behavior of the system (see Figure 7). However the value of several key parameters, namely the magnetization M of the micro-object and the viscous coefficient h, must be determined to get a numerical model to design closed loop control. This section

TABLE I: Values of the steady state position X_∞, the magnetic field gradient ∇B_{moy} in the workspace and the magnetization M for different values of the current. $R_c = 10.5$ mm (measured from a side view of the system), $\rho_{Nickel} = 8902$ kg/m^3.

I(A)	∇B_{moy}(T/m)	X_∞(µm)	M(A/m)
0.26	0.26	52	1661
0.32	0.33	98	2467
0.40	0.39	157	3344
0.47	0.47	283	4898

presents a method for the identification of these parameters based on the experimental measurements performed on the large object 100x90x25 µm^3 in open loop. This set of data has been selected since it has a pretty good repeatability. Data from the Section II are used and additional experiments are performed to obtain measurements for several values of I.

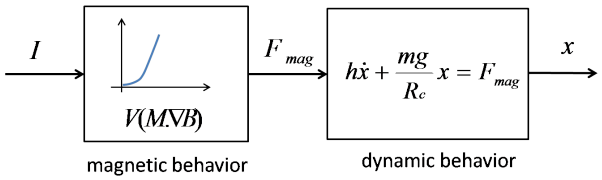

Fig. 7: These two subsystems illustrate the relation between the input of the system I (current set to the electromagnets) and the output of the system x (position of the object).

A. Identification of the magnetic behavior

The magnetization M of the micro-object is a key parameter, which varies a lot depending on the properties of the object and its fabrication process. Its value cannot be directly obtained in the literature. However it can be identified based on Eq. (11) and on the experimental measurements. Table I presents the values of M for several magnitudes of current. The identified values depend on I but remain below the saturation of the nickel material (4.7 10^5 A/m according to [52]). The magnetic force is non linear with respect to I and can be approximated by the following expression for the typical range of current used for this magnetic device:

$$\tilde{F}_{mag}(I) = kVI^2, \tag{13}$$

where $k = 3750$ T/Am^2.

This relation enables to obtain the analytical relation between the input current I and the magnetic force applied to the micro-object (first bloc of Figure 7). This relation can be easily inverted in order to linearise the system for closed loop control. Thus, the current I is expressed in function of the estimated magnetic force by the relation:

$$I = \sqrt{\frac{\tilde{F}_{mag}}{kV}}, \tag{14}$$

B. Identification of the dynamic behavior - viscous coefficient

The dynamic behavior of the micro-object depends on the values of some key parameters, namely R_c, m and h. The radius of curvature R_c can be estimated from side view images of the setup. In addition the mass of the object m can be calculated through the value of the density of the material founded in literature and the dimensions of the object measured under a microscope. The viscous coefficient is however an unknown parameter in the dynamic model, which is not easily found in the literature since it varies greatly depending on the shape of the object. The value of this parameter is identified using the same methodology as in [53]. The results are presented in Table II for several values of the input current, based on the equation (12). As predicted by Eq. (12) its value does not depend on the input current. The average value of the viscous coefficient is $h = 3.39\ 10^{-7}$ kg/s. It can be noted that this coefficient does not depend on the velocity of the micro-object. The computation of the Reynolds number R_e indeed confirms the assumption of Stokes flow since $R_e < 1$. The identified value of the viscous coefficient enables the complete definition of the numerical model of the dynamic behavior of the micro-object.

TABLE II: Experimental measurements of the response time τ for different input currents I. The viscous coefficient h and the Reynolds number R_e are computed based on these measures for $\rho_{Nickel} = 8902$ kg/m^3 and a measured radius of curvature of the meniscus of $R_c = 10.5$ mm.

I(A)	τ(ms)	h(kg/s)	R_e
0.26	194	$3.63\ 10^{-7}$	0.15
0.32	178	$3.32\ 10^{-7}$	0.17
0.40	181	$3.37\ 10^{-7}$	0.16
0.47	174	$3.24\ 10^{-7}$	0.17

C. Validation of the model

Using the parametric approximation of the magnetic force determined in Sec. IV-A and the viscous coefficient $h = 3.39\ 10^{-7}$ kg/s identified in Sec. IV-B the dynamic model Eq. (10) of the micro-object behavior is simulated. Figure 8 provides a comparison between the simulation and the experimental measurements of the position response for several current values. The trends of the simulated and experimental plots are similar.

The assumptions assumed in Sec. III-B are indeed verified:

- From side view images of the reservoir it has been verified that the shape of the meniscus is spherical (see Figure 3).
- The magnetic force induces only local displacements around the center of the workspace. From the experimental measurements it has been estimated that the displacement to reach the steady state position X_∞ is around 35 times smaller than the value of the radius of curvature R_c.
- The plots of the position measurements (see Figure 4(a) for example) are typical of a first order system, for

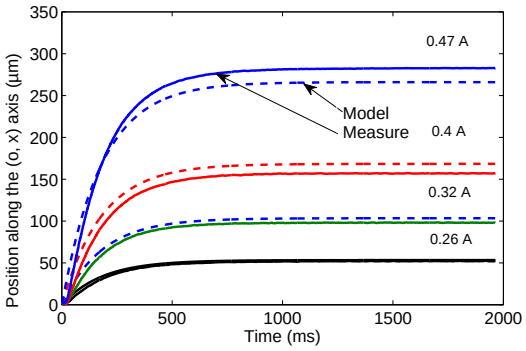

Fig. 8: Comparison between the simulated and the experimental responses. The numerical values used in the simulation are the following: $R_c = 10,5$ mm, $\rho = 8902$ kg/m^3.

which the velocity is not continuous. They confirm that the inertia of the object can be neglected.

The differences between the model and the experiments come from different sources, among which is the variation of the radius of curvature of the meniscus R_c. This value varies for each refilling process. Based on the measurements of the steady state position in Fig. 5(b) and the equation Eq. 11, the radius of curvature of the meniscus ranges from 8.7 mm and 11.4 mm. This corresponds to a variation of 3 degrees of the contact angle, which is in good agreement with what is presented in [47]. Therefore, the uncertainty $\frac{\Delta X}{X_\infty}$ of the position using the identified model is about 16 %. This implies some inaccuracies in the identification of the viscous coefficient and the magnetization.

The use of a VSM (Vibrating Sample Magnetometer) would allow more accurate measurements of the magnetization. The accuracy of the dynamic model of the object would be enhanced. It can be interesting to use a VSM when the magnetic objects are controlled in open loop since a fine modeling of the magnetic behavior is required in this case. However, if the object is controlled in closed loop an accurate dynamic model in not required which justify the use of the position measurements to identify the values of the magnetization. Therefore, the present model is used in the next section for closed loop control of the object's position.

D. Performance analysis

To compare the velocity that can be reached at the air/liquid interface to the one that would have been reached in similar conditions inside the liquid a numerical simulation has been performed using a finite element software, Comsol Multiphysics 4.2. To perform this comparison the key element is the drag coefficient that would experience the particle inside the liquid. To determine it we have performed a numerical simulation based on an object of size 100x90x25 µm^3. The object is considered stationary between two plates where the distance between the two plates is equal to 5 mm. It experiences a fluidic flow. The velocity of the fluid used in this simulation is such that the Reynolds number remains lower than 1 so that the Stokes law is valid.

Based on this simulation the viscous coefficient of the micro-object immersed inside water is equal to 2.210^{-6} kg/s. This value is about 10 times larger than the identified value h (see Eq. 10) which means that the velocity of the micro-object on the air/water interface should theoretically be 10 times larger than inside water. However, magnetic actuation inside liquids with velocities higher than what is obtained here are reported. In particular, in [54] they performed trajectories at 556 µm/s. This result is however obtained for an object almost 10 times larger (400 µm). High velocities are also reported in ambient environments. For example the velocity can reach 133 mm/s in [30]. However, the behavior of the micro-objects is less repeatable because of the adhesion forces, and precise positioning is difficult. Compared to the approaches proposed in literature this work enables to get both high velocities and precise positioning for objects of around 50 µm. This is thus a good trade off between velocity and precision.

V. Position control

Closed loop control is performed based on the model given in the previous sections. The behavior of an object is characterized by its non linearity with respect to the applied current I. Indeed, the equation (13) show that the magnetic force F_{mag} depends on the square of the current I. To design a linear controller, it is necessary to linearise the system by introducing the estimated magnetic force $\tilde{F}_{mag}$ as a new control variable. The coefficient of the linear controller will be identified based on the new linear model where $\tilde{F}_{mag}$ is the input of the system and x is the output of the system. In this case, the control law proposed can be illustrated by two blocks (see Figure 9). The first bloc is a linear controller (proportional-integral: PI or proportional-derivative: PD according to the desired trajectory) which computes the necessary magnetic force $\tilde{F}_{mag}$ to be applied to the micro-object. In a second step the current I to be sent by the electronic amplifier is calculated based on the relation given by Eq. (14).
The behavior of the small objects is sensitive to the variability of the meniscus geometry. The closed loop control should guarantee a precise positioning despite these perturbations. In addition, it is also tested for tracking trajectories to demonstrate high speed motion of the objects at the air/water interface.

A. Closed loop control for precise positioning

Closed loop control is implemented to guarantee a precise positioning of micrometer size objects. The proposed control law is based on a proportional integrator controller. Several experiments have been performed on the medium size object (60x50x25 µm^3) either for a constant or a variable meniscus. Initially the micro-object is at the position $x = 0$ µm. The desired position is fixed at $x = 250$ µm. To calculate the adequate magnetic forces, the parameters of the PI controller are chosen

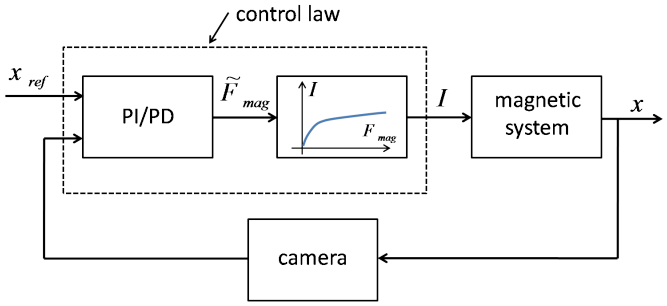

Fig. 9: Schematic of the closed loop control of the position of the micro-object

to obtain a position response of a first order dynamic behavior. Based on the identified model the coefficients are expressed by:

$$\begin{cases} K_p = \dfrac{mg}{R_c}\left(\dfrac{\tau}{\tau_{BF}}\right), \\ \tau_i = \tau, \end{cases} \tag{15}$$

where K_p is the proportional coefficient, τ_i is the integration coefficient, τ_{BF} is the desired response time in closed loop mode and g is the acceleration of the gravity. The desired response time is chosen equal to 200 ms. Thus, the proportional coefficient is equal to 1.4 10^{-6} mN^{-1} and the integration constant is equal to the approximated time constant of the open loop behavior 450 ms.

Figure 10(a) shows the position response of the micro-object using closed loop control. The meniscus is constant for the three different trials since no re-filling has been performed between each trial. Closed loop control improves the repeatability as it can be seen by comparing these plots to the ones of Figure. 5(b).

The proposed closed loop is also tested to reject the disturbance introduced by the variation of the meniscus shape. Three experiments have been performed on the same 60x50x25 μm^3 object. After each experiment the container is emptied and re-filled in order to obtain different shapes of the meniscus for each experiment. Figure 10(b) shows the position response of the micro-object. It can be seen that in the case with no refilling the repeatability is indeed better than when the reservoir is refilled. This is due indeed to the variations of the meniscus.

However good precision is obtained with and without refilling since the position error between the experimental position and the desired position is less than 4 % of the object size. This result shows the ability to control precisely the position of a small object rejecting the disturbances.

As shown in Figure 10, overtaking sometimes occurs. It is not due to inertia since that would mean that it would be present on all the plots. In addition, based on the plots the maximum inertia force is about 3.75 10^{-13} N which is 3

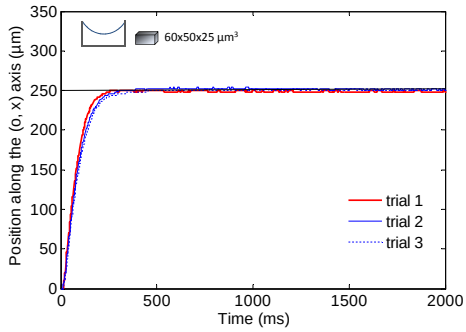

(a) Position response for three different trials performed with a constant meniscus.

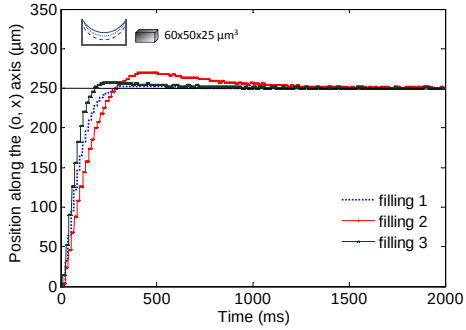

(b) Position response for three different trials. The reservoir is re-filled between each experiments.

Fig. 10: Closed loop control of the 60x50x25 μm^3 object with either a constant or a variable meniscus. The position error between the desired and the experimental position is less than 4 % of the object size.

orders of magnitude lower than the magnetic force applied (about 1.69 10^{-10} N). The overtaking is rather introduced by the controller. The coefficients of the controller have been set constant. However, since the meniscus varies overtaking occurs sometimes.

This control law is also tested on the 30x20x25 μm^3 object. The desired position is also fixed at $x = 250$ µm. The proportional constant of the PI controller is equal to 2.4 10^{-7} mN^{-1} and the integration constant is equal to 780 ms, which ensure a response time equal to 400 ms. Figure 11 shows the position response. The position error between the desired and the experimental position is less than 7 % of the object size. Additional experiments have been performed for a shorter response time (200 ms) and demonstrate also a good positioning of the micro-object.

Closed loop control does indeed enable to guarantee a precise positioning despite the variation of the meniscus and the small size of the objects.

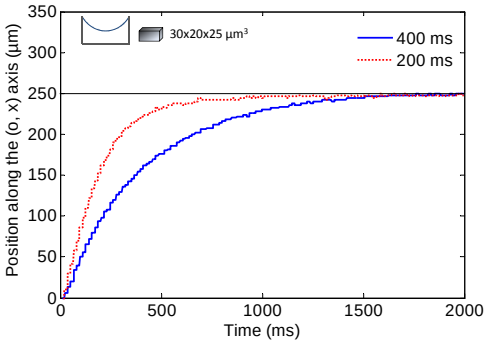

Fig. 11: Position response for two different trials (the desired response time is respectively 400 ms and 200 ms). The position error between the experimental position and the desired position is less than 7 % of the object size.

B. Closed loop control for 1D trajectory tracking

To control the trajectory of a small object along the (o,x) axis, a new control law is implemented to track a sinusoidal trajectory. This control law is based on the use of a proportional derivative controller on the first bloc of control to improve the rapidity. The motion is ensured by two electromagnets located in the same axis opposite each other. To track high dynamic trajectories, each electromagnet is moved closer to the workspace in order to increase the magnetic field gradient and thus increase the velocity of objects. The model presented in Section. III is identified for electromagnets placed 9 mm away from the workspace center. The experiments presented here are performed at a distance equal to 5 mm. To evaluate the influence of this parameter on the performance of closed loop control, the previous identification is used in this new configuration.

Two experiments are performed on the 60x50x25 μm^3 object. Firstly, the proposed control law has been tested on low speed trajectory, a sinusoidal trajectory with 500 ms period and a magnitude of 100 µm around workspace center (Figure 13(a)). The error between the experimental trajectory and the reference is less than 7 µm which represents 4 % of the micro-object size and the maximum velocity achieved is about 1.25 mm/s.

Secondly, the control law proposed is tested for a high speed trajectory, a sinusoidal trajectory 5 times faster (Figure 13(b)). As seen in the figure, the micro-object starts its motion after a delay of 6 ms. This is due to the fact that it first rotates around its center of mass to align its magnetization vector with the magnetic field (see Figure 12). The same rotation occurs each time the direction of motion change. The same phenomena does appear in Figure 13(a) but can hardly be seen due to the time scale of the figure. This rotation can be avoided by powering the two electromagnets with a current of opposite sign.

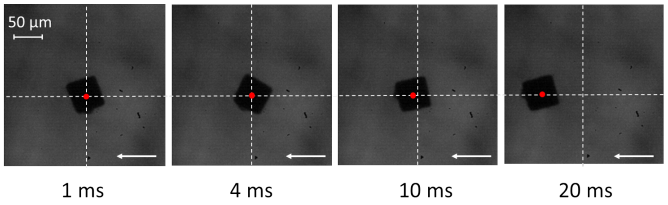

Fig. 12: Before moving the micro-object first rotates to align the magnetization vector and the direction of the magnetic field. This rotation also occurs each time the direction of motion is changed. The arrows indicate the direction of the magnetic field.

At the time $t = 6$ ms the objects starts to follow the reference trajectory. The position error is less than 10 % of the object size and the maximum velocity achieved is about 6 mm/s. To further minimize the position error, additional tests are performed by increasing the proportional coefficient but instability occur. An advanced control strategy should be used but is beyond the scope of this present study.

These results demonstrate that the closed loop control can track precisely high speed trajectories.

VI. Discussion

A. Increase of the velocity

In order to further increase the velocity, several directions can be foreseen. One solution consists in increasing the magnetic force by changing the dimensions of the electromagnets, or by moving them closer to the workspace. If they are placed 2 mm away from the workspace center the magnetic field gradient will be about 8 T/m. This value is 3 times higher than the values of the magnetic field gradient produced when the electromagnets are placed at 5 mm. In this case, the velocity of a 60x50x25 μm^3 object can increase from 6 mm/s to 18 mm/s.

Another solution is to use hydrophobic coatings. Indeed, at the air/liquid interface, the shear coefficient depends on the viscosity of the liquid, the geometry of the object and the contact angle between the object and the liquid surface [51]. Using hydrophobic coatings can reduce the contact angle between the object and the liquid surface and then reduce the drag force. The contact surface between the object and the liquid can also be reduced. Indeed the viscous coefficient decreases with the reduction of the contact surface. A new design where three beads of 1 μm^3 are attached to a 60x50x25 μm^3 object can be considered. The beads will be in contact with the liquid surface and should present a surface tension able to compensate the weight force. The value of the viscous coefficient h should be reduced 20 times. The actuation speed is not perfectly proportional to the resistance and the drive force. However, at this scale it is a fairly good approximation since the inertia can be neglected. Thus, the velocity of the micro-object should be 20 times faster.

TABLE III: Values of the velocity and the precision error on the literature, for objects less than 100 µm the velocity reached is less than 0.3 mm/s with a precision error of tens of micrometer.

Ref	size (µm)	medium	DDL	control	precision (µm)	velocity (mm/s)	velocity (*body legth*/s)
[54]	500	liquid	1D	open loop	.	556	1112
[30]	388x388x230	air	1D	open loop	.	133	342.8
Present work	60x50x25	air/liquid	1D	closed loop	< 6	6	100
[19]	300x300x70	liquid	2D	open loop	.	12.5	41.6
[29]	250x130x100	liquid	2D	open loop	.	10	40
[37]	42	liquid	2D	closed loop	30	0.3	7.14
[55]	500x375x250	liquid	3D	closed loop	.	1.9	3.8
[23]	300x60x50	liquid	2D	open loop	.	~ 1	~ 3.33
[38]	50	liquid	2D	closed loop	33	0.158	3.16
[56]	350	liquid	3D	closed loop	310	< 1	< 2.85
[31]	100	liquid	2D	closed loop	48 ± 59	0.279	2.79
[57]	$60-110$	air/liquid	2D	closed loop	8.4	0.235	2.13
[58]	500	liquid	2D	open loop	.	0.710	1.42
[59]	10	liquid	3D	.	.	0.01	1
[33]	30x30x10	liquid	2D	open loop	.	0.02	0.66
[45]	$100-200$	liquid/liquid	2D	closed loop	$4.1-40.5$	0.023	$0.11-0.23$

This study is thus only the first step toward very high speed motion and demonstrates the benefit of the air/liquid interface for fast displacements.

B. From the proof of concept to the first prototype

To go from the proof of concept of high speed motion at the air/liquid interface to a smart surface for high speed conveying of microcomponents will necessitate to address several technical issues.

In future works, a new strategy of control will be developed to control the trajectory of the micro-objects in 2D for long distance and high speed. This strategy will be based on the combination of two controllers; one controller for the motion along the (o, x) axis and one controller for the motion along the (o, y) axis. The velocity of the object should be the superposition of the velocity along the two axes. Thus, the maximum velocity of the object when it moves outside the reference axis will be larger than the one along the reference axis. To further increase the velocity of the object, the electromagnets will be moved closer to the workspace. In this case, the non linearity of the magnetic field is not negligible and the magnetic coupling between the electromagnets must be taken into account. A new model including these issues will be developed.

In addition, long range displacements will introduce a variation of the vertical position of the object due to the meniscus, which can be an issue for the visual feedback since depth of field of high magnification objectives of microscopes are limited. In that case it is possible to place the camera on a micropositioning motor to servo the vertical position of the camera using an autofocusing technique to ensure a correct focus of the images.

There are several sources of evaporation of the fluid, among which the lighting elements and the electromagnetic coils. If experiments longer than an hour have to be performed a refilling of the reservoir is necessary with the current system. Two approaches can be foreseen to avoid any inconvenience due to this operation: (i) using a liquid with long evaporation time (such as organic oil for example), (ii) using a fluidic setup that will perform continuous refilling controlled by the height of the liquid in the reservoir. Since the flow rates will be small there should not be too much perturbations of the air/liquid interface if the height of the reservoir is sufficient and if the fluid is injected at the bottom of the reservoir. However this will not ensure a constant meniscus angle because of the capillary hysteresis produced by the roughness of the container material and chemical imperfections [60]. Closed loop control will still be necessary to ensure a correct positioning of the particles.

C. Range of object size for actuation at the air/liquid interface

Two conditions must be respected to ensure the applicability of the smart surface actuation:

- The weight of the micro-object must be compensated by the resultant force of the surface tension so that the object does not sink,
- The force used to pick up the micro-objects from the air/liquid interface after the conveying must be larger than the resultant of the surface tension.

The first condition benefits from the small dimension of the object. Indeed the weight is proportional to the volume V of the object: $P = \rho g V$ where ρ is its density and g is the acceleration of gravity. The resultant of the surface tension

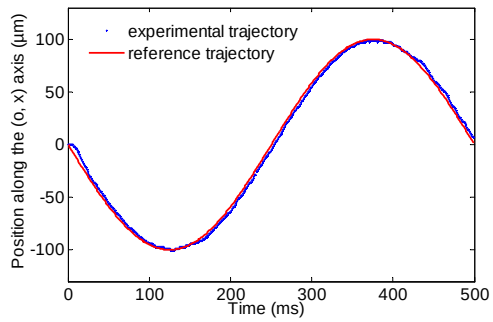

(a) Experimental trajectory of the micro-object while tracking a sinusoidal trajectory of 500 ms period. The proportional constant is equal to 7 10^{-6} mN^{-1} and the derivative constant is equal to 57 ms.

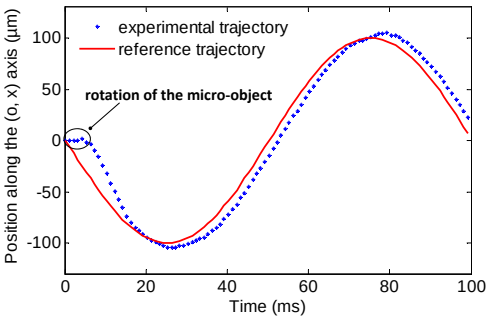

(b) Experimental trajectory of the micro-object while tracking a sinusoidal trajectory of 100 ms period. The proportional constant is equal to 1.2 10^{-5} mN^{-1} and the derivative constant is equal to 72 ms.

Fig. 13: Experimental closed loop trajectory tracking. These experiments are performed using the 60x50x25 μm^3 object. The camera acquisition period is 1 ms. During the first six milliseconds the object rotate to align its magnetization and the magnetic field.

$\vec{T}$ is a linear force proportional to the size of the object (see Figure 6). The maximum force T_{max} is given by: $T_{max} = \gamma C$, where C is the perimeter of the object and γ is the surface tension. Considering a cubic object with a side length d a critical upper limit dimension d_{cr} can be obtained when the two forces are equal (the weight can be neglected):

$$T_{max} \geq P \implies d_{cr} = \sqrt{\frac{4\gamma}{\rho g}}. \tag{16}$$

For a nickel object placed on water ($\rho = 8902$ kg/m^3, $\gamma = 72$ 10^{-3} N/m) a critical dimension of 1.8 mm is obtained, which justifies the capacity to maintain objects in equilibrium on the liquid surface at microscale.

To pick-up the objects from the liquid surface a vacuum gripper can be used as in [61] where they handled 100 µm sized diamonds or in [62] where they work with ultra-thin 10 µm dies provided that the objects are not porous. For example, to pick up a cubic object with a side length d with a vacuum gripper with an outer diameter d, the necessary pressure p is defined as follows:

$$p = \frac{T_{max}}{\pi\left(\frac{d}{2}\right)^2}, \tag{17}$$

In that case the dimension of the object must be larger than:

$$p_{atm} \geq p \implies d \geq \frac{16\gamma}{\pi p_{atm}}, \tag{18}$$

where p_{atm} is the atmospheric pressure. If the liquid considered is water the objects must have a dimension d larger than 1.4 µm.

D. Interaction with non magnetic objects

All this work deals with the transportation of magnetic objects. If non magnetic ones must be conveyed several solutions can be foreseen. One possible solution consists in attaching magnetic parts to the objects. A second one is to use magnetic particles to create a circulation of the liquid (like vortex pumps) as demonstrated in [44] at the air/liquid interface using holographic tweezers. Another solution can consist in pushing the objects, or approaching them to grip them. However, in that case the interactions will be highly influenced by surface tension effects as mentioned in [22], [63].

VII. Conclusion

This paper demonstrates the ability to move a micro-object at the air/liquid interface using magnetic actuation. Based on open loop experiments, the repeatability of the behavior of objects is studied. A model of the dynamic behavior of the micro-objects on the meniscus has been built, and the physical parameters (their magnetization and their viscous coefficient) have been identified. A closed loop control based on the identified model is implemented to control the position of objects. It demonstrates a precise positioning and high speed motion of objects smaller than 100 µm. The position error of an object of 60x50x25 μm^3 is less than 10 % of its size and the maximum velocity reached is about 6 mm/s. The position error of an object of 30x20x25 μm^3 is less than 7 % of its size. Compared to the current approaches proposed in the literature, this approach contributes to increase the velocity of displacement and the precision of the positioning of objects smaller than 100 µm. It is the first step toward magnetic smart surfaces at the micrometer scale which will enable high throughput transportation and precise positioning of micrometer size objects. It is of crucial interest for the design of future micro assembly lines.

Acknowledgements

This work has been supported by the French Agence Nationale de la Recherche, through the LEMA project (contract

"ANR 12 BS03 007 01"), by the Labex ACTION project (contract "ANR-11-LABX-01-01"), by the "Région Franche-comté" and by the French RENATECH network and its FEMTO-ST technological facility.

REFERENCES

[1] I. Georgilas, A. Adamatzky, and C. Melhuish, "Towards an intelligent distributed conveyor," in *Advances in Autonomous Robotics*. Springer, 2012, pp. 457–458.

[2] A. Delettre, G. J. Laurent, Y. Haddab, and N. Le Fort-Piat, "Robust control of a planar manipulator for flexible and contactless handling," *Mechatronics*, vol. 22, no. 6, pp. 852–861, 2012.

[3] D. El Baz, V. Boyer, J. Bourgeois, E. Dedu, and K. Boutoustous, "Distributed part differentiation in a smart surface," *Mechatronics*, vol. 22, no. 5, pp. 522–530, 2012.

[4] C. Pawashe, S. Floyd, E. Diller, and M. Sitti, "Two-dimensional autonomous microparticle manipulation strategies for magnetic microrobots in fluidic environments," *IEEE Transactions on Robotics*, pp. 467–477, 2012.

[5] M. Hagiwara, T. Kawahara, T. Iijima, Y. Yamanishi, and F. Arai, "High speed microrobot actuation in a microfluidic chip by levitated structure with riblet surface," in *IEEE International Conference on Robotics and Automation*, 2012, pp. 2517–2522.

[6] A. Chen, T. Byvank, W.-J. Chang, A. Bharde, G. Vieira, B. L. Miller, J. J. Chalmers, R. Bashir, and R. Sooryakumar, "On-chip magnetic separation and encapsulation of cells in droplets," *Lab on a Chip*, 2013.

[7] T. Yue, M. Nakajima, H. Tajima, and T. Fukuda, "Fabrication of microstructures embedding controllable particles inside dielectrophoretic microfluidic devices," *International journal of advanced robotic systems*, vol. 10, 2013.

[8] S.-W. Nam, S. H. Kim, J.-K. Park, and S. Park, "Dielectrophoresis in a slanted microchannel for separation of microparticles and bacteria," *Journal of nanoscience and nanotechnology*, vol. 13, no. 12, pp. 7993–7997, 2013.

[9] M. Kharboutly, M. Gauthier *et al.*, "High speed closed loop control of a dielectrophoresis-based system." in *IEEE International Conference on Robotics and Automation*, 2013, pp. 1438–1443.

[10] M. Kharboutly, M. Gauthier, and N. Chaillet, "Modeling the trajectory of a microparticle in a dielectrophoresis device," *Journal of Applied Physics*, vol. 106, no. 11, p. 114312, 2009.

[11] S. Chen, J. Cheng, C.-W. Kong, X. Wang, S. H. Cheng, R. A. Li, and D. Sun, "Laser-induced fusion of human embryonic stem cells with optical tweezers," *Applied Physics Letters*, vol. 103, no. 3, p. 033701, 2013.

[12] S. Chowdhury, A. Thakur, P. Svec, C. Wang, W. Losert, and S. K. Gupta, "Automated manipulation of biological cells using gripper formations controlled by optical tweezers," *IEEE Transactions on Automation Science and Engineering*, vol. 11, no. 2, pp. 338–347, April 2014.

[13] C. Pacoret and S. Régnier, "Invited article: A review of haptic optical tweezers for an interactive microworld exploration," *Review of Scientific Instruments*, vol. 84, no. 8, p. 081301, 2013.

[14] J. Lei, P. Glynne-Jones, and M. Hill, "Acoustic streaming in the transducer plane in ultrasonic particle manipulation devices," *Lab Chip*, vol. 13, no. 11, pp. 2133–2143, 2013.

[15] D. Foresti, M. Nabavi, M. Klingauf, A. Ferrari, and D. Poulikakos, "Acoustophoretic contactless transport and handling of matter," *Bulletin of the American Physical Society*, vol. 58, 2013.

[16] H. Marino, C. Bergeles, and B. J. Nelson, "Robust electromagnetic control of microrobots under force and localization uncertainties," *IEEE Transactions on Automation Science and Engineering*, vol. 11, no. 1, pp. 310 – 316, 2014.

[17] Z. Ye and M. Sitti, "Dynamic trapping and two-dimensional transport of swimming microorganisms using a rotating magnetic microrobot," *Lab Chip*, vol. 14, pp. 2177–2182, 2014.

[18] K. Belharet, D. Folio, and A. Ferreira, "Three-dimensional controlled motion of a microrobot using magnetic gradients," *Advanced Robotics*, vol. 25, no. 8, pp. 1069–1083, 2011.

[19] D. R. Frutiger, K. Vollmers, B. E. Kratochvil, and B. J. Nelson, "Small, fast, and under control: wireless resonant magnetic micro-agents," *The International Journal of Robotics Research*, vol. 29, no. 5, pp. 613–636, 2010.

[20] E. B. Steager, M. S. Sakar, C. Magee, M. Kennedy, A. Cowley, and V. Kumar, "Automated biomanipulation of single cells using magnetic microrobots," *The International Journal of Robotics Research*, vol. 32, no. 3, pp. 346–359, 2013.

[21] B. Véron, J. Abadie, A. Hubert, N. Andreff *et al.*, "Magnetic manipulation with several mobile coils towards gastrointestinal capsular endoscopy." *New Trends in Mechanism and Machine Science. Theory and Applications in Engineering.*, pp. 681–690, 2012.

[22] Z. Ye, E. Diller, and M. Sitti, "Micro-manipulation using rotational fluid flows induced by remote magnetic micro-manipulators," *Journal of Applied Physics*, vol. 112, no. 6, pp. 064 912–064 912, 2012.

[23] H.-W. Tung, K. E. Peyer, D. F. Sargent, and B. J. Nelson, "Noncontact manipulation using a transversely magnetized rolling robot," *Applied Physics Letters*, vol. 103, no. 11, p. 114101, 2013.

[24] K. E. Peyer, L. Zhang, and B. J. Nelson, "Bio-inspired magnetic swimming microrobots for biomedical applications," *Nanoscale*, vol. 5, no. 4, pp. 1259–1272, 2013.

[25] T. Xu, G. Hwang, N. Andreff, and S. Régnier, "Modeling and swimming property characterizations of scaled-up helical microswimmers," *Transactions on Mechatronics*, 2013.

[26] I. S. Khalil, M. P. Pichel, L. Zondervan, L. Abelmann, and S. Misra, "Characterization and control of biological microrobots," in *Experimental Robotics*. Springer, 2013, pp. 617–631.

[27] S. Martel, "Bacterial microsystems and microrobots," *Biomedical microdevices*, vol. 14, no. 6, pp. 1033–1045, 2012.

[28] D. H. Kim, P. S. S. Kim, A. A. Julius, and M. J. Kim, "Three-dimensional control of engineered motile cellular microrobots," in *IEEE International Conference on Robotics and Automation*, 2012, pp. 721–726.

[29] C. Pawashe, S. Floyd, and M. Sitti, "Modeling and experimental characterization of an untethered magnetic micro-robot," *The International Journal of Robotics Research*, vol. 28, no. 8, pp. 1077–1094, 2009.

[30] I. A. Ivan, G. Hwang, J. Agnus, M. Rakotondrabe, N. Chaillet, and S. Régnier, "First experiments on magpier: a planar wireless magnetic and piezoelectric microrobot," in *IEEE International Conference on Robotics and Automation*, 2011, pp. 102–108.

[31] I. S. Khalil, V. Magdanz, S. Sanchez, O. G. Schmidt, and S. Misra, "The control of self-propelled microjets inside a microchannel with time-varying flow rates," *Transactions on Robotics*, vol. 30, no. 1, pp. 49–58, 2014.

[32] I. S. Khalil, J. D. Keuning, L. Abelmann, and S. Misra, "Wireless magnetic-based control of paramagnetic microparticles," in *IEEE International Conference on Biomedical Robotics and Biomechatronics*, 2012, pp. 460–466.

[33] M. S. Sakar, E. B. Steager, A. Cowley, V. Kumar, and G. J. Pappas, "Wireless manipulation of single cells using magnetic microtransporters," in *IEEE International Conference on Robotics and Automation*, 2011, pp. 2668–2673.

[34] I. S. Khalil, V. Magdanz, S. Sanchez, O. G. Schmidt, and S. Misra, "Three-dimensional closed-loop control of self-propelled microjets," *Applied Physics Letters*, vol. 103, no. 17, p. 172404, 2013.

[35] W. Sun, I. S. Khalil, S. Misra, and R. Alterovitz, "Motion planning for paramagnetic microparticles under motion and sensing uncertainty," in *IEEE International Conference on Robotics and Automation*, 2014.

[36] I. S. Khalil, P. Ferreira, R. Eleutério, C. L. de Korte, and S. Misra, "Magnetic-based closed-loop control of paramagnetic microparticles using ultrasound feedback," in *IEEE International Conference on Robotics and Automation*, 2014.

[37] A. Barbot, D. Dominique, and H. Gilgueng, "Controllable roll-to-swim motion transition of helical nanoswimmers," in *IEEE International Conference on Robotics and Automation*, 2014.

[38] S. M. I. Khalil, Y. Kareem, S. Alonso, and M. Sarthak, "Magnetic-based motion control of sperm-shaped microrobots using weak oscillating magnetic field," in *IEEE International Conference on Intelligent Robots and Systems*, 2014.

[39] S. Bouchebout, A. Bolopion, M. Kharboutly, I. A. Ivan, J. Agnus, and S. Régnier, "Design and first experiments on magpier, the magnetic microrobot," in *IEEE International Symposium on Optomechatronic Technologies*, 2012.

[40] M. Gauthier, S. Régnier, P. Rougeot, and N. Chaillet, "Analysis of forces for micromanipulations in dry and liquid media," *Journal of Micromechatronics*, vol. 3, no. 3-4, pp. 3–4, 2006.

[41] S. Gupta, N. Singh, M. Sastry, R. Kakkar, and R. Pasricha, "Controlling the assembly of hydrophobized gold nanoparticles at the air–water interface by varying the interfacial tension," *Thin Solid Films*, vol. 519, no. 3, pp. 1072–1077, 2010.

[42] J. M. Ng, M. J. Fuerstman, B. A. Grzybowski, H. A. Stone, and G. M. Whitesides, "Self-assembly of gears at a fluid/air interface," *Journal of the American Chemical Society*, vol. 125, no. 26, pp. 7948–7958, 2003.

[43] P. Rogers, I. Gralinski, C. Galtry, and A. Neild, "Selective particle and cell clustering at air–liquid interfaces within ultrasonic microfluidic

systems," *Microfluidics and nanofluidics*, vol. 14, no. 3-4, pp. 469–477, 2013.
[44] A. Jesacher, S. Fürhapter, C. Maurer, S. Bernet, and M. Ritsch-Marte, "Holographic optical tweezers for object manipulations at an air-liquid surface," *Optics express*, vol. 14, no. 13, pp. 6342–6352, 2006.
[45] J. A. Piepmeier, S. Firebaugh, and C. S. Olsen, "Uncalibrated visual servo control of magnetically actuated microrobots in a fluid environment," *Micromachines*, vol. 5, no. 4, pp. 797–813, 2014.
[46] M. Dkhil, A. Bolopion, M. Gauthier, and S. Régnier, "Modeling and experiments of high speed magnetic micromanipulation at the air/liquid interface," in *IEEE International Conference on Intelligent Robots and Systems*, 2014.
[47] C. Della Volpe, D. Maniglio, S. Siboni, and M. Morra, "An experimental procedure to obtain the equilibrium contact angle from the wilhelmy method," *Oil & gas science and technology*, vol. 56, no. 1, pp. 9–22, 2001.
[48] O. Pitois and X. Chateau, "Small particle at a fluid interface: Effect of contact angle hysteresis on force and work of detachment," *Langmuir*, vol. 18, no. 25, pp. 9751–9756, 2002.
[49] C. Lam, N. Kim, D. Hui, D. Kwok, M. Hair, and A. Neumann, "The effect of liquid properties to contact angle hysteresis," *Colloids and Surfaces A: Physicochemical and Engineering Aspects*, vol. 189, no. 1, pp. 265–278, 2001.
[50] M. Gauthier and M. Nourine, "Capillary force disturbances on a partially submerged cylindrical micromanipulator," *IEEE Transactions on Robotics*, vol. 23, no. 3, pp. 600–604, 2007.
[51] J. T. Petkov, N. D. Denkov, K. D. Danov, O. D. Velev, R. Aust, and F. Durst, "Measurement of the drag coefficient of spherical particles attached to fluid interfaces," *Journal of colloid and interface science*, vol. 172, no. 1, pp. 147–154, 1995.
[52] K. Mulyokov, G. Korznikov, R. Abdulov, and R. Valiev, "Magnetic hysteretic properties of submicron grained nickel and their variations upon annealing," *Journal of magnetism and magnetic materials*, vol. 89, no. 1-2, pp. 207–213, 1990.
[53] J. T. Petkov, N. D. Denkov, K. D. Danov, O. D. Velev, R. Aust, and F. Durst, "Measurement of the drag coefficient of spherical particles attached to fluid interfaces," *Journal of colloid and interface science*, vol. 172, no. 1, pp. 147–154, 1995.
[54] H. Salmon, L. Couraud, and G. Hwang, "Swimming property characterizations of magnetic polarizable microrobots," in *IEEE International Conference on Robotics and Automation*, 2013.
[55] M. P. Kummer, J. J. Abbott, B. E. Kratochvil, R. Borer, A. Sengul, and B. J. Nelson, "Octomag: An electromagnetic system for 5-dof wireless micromanipulation," *IEEE Transactions on Robotics*, pp. 1006–1017, 2010.
[56] E. Diller, J. Giltinan, and M. Sitti, "Independent control of multiple magnetic microrobots in three dimensions," *The International Journal of Robotics Research*, vol. 32, no. 5, pp. 614–631, 2013.
[57] J. D. Keuning, J. de Vriesy, L. Abelmanny, and S. Misra, "Image-based magnetic control of paramagnetic microparticles in water," in *IEEE International Conference on Intelligent Robots and Systems*, 2011, pp. 421–426.
[58] S. Palagi, G. Lucarini, V. Pensabene, A. Levi, B. Mazzolai, A. Menciassi, and L. Beccai, "Wireless swimming microrobots: Design and development of a 2 DoF magnetic-based system," in *IEEE International Conference on Robotics and Automation*, 2012, pp. 3455–3460.
[59] S. Schurle, K. E. Peyer, B. Kratochvil, and B. J. Nelson, "Holonomic 5-DOF magnetic control of 1D nanostructures," in *IEEE International Conference on Robotics and Automation*, 2012, pp. 1081–1086.
[60] W. Chesworth, *Encyclopedia of Soil Science*. Springer, 2008, p. 86.
[61] W. Zesch, M. Brunner, and A. Weber, "Vacuum tool for handling microobjects with a nanorobot," in *IEEE International Conference on Robotics and Automation*, vol. 2, 1997, pp. 1761–1766.
[62] V. Liimatainen, M. Kharboutly, D. Rostoucher, M. Gauthier, and Q. Zhou, "Capillary self-alignment assisted hybrid robotic handling for ultra-thin die stacking," in *International Conference on Robotics and Automation*. IEEE, 2013, pp. 1403–1408.
[63] S. Miyashita, E. Diller, and M. Sitti, "Two-dimensional magnetic micromodule reconfigurations based on inter-modular interactions," *The International Journal of Robotics Research*, vol. 32, no. 5, pp. 591–613, 2013.